# Mechanism of lid closure in the eukaryotic chaperonin TRiC/CCT

**Christopher R Booth**[1,2,5], **Anne S Meyer**[3,5], **Yao Cong**[2], **Maya Topf**[4,5], **Andrej Sali**[4], **Steven J Ludtke**[1,2], **Wah Chiu**[1,2], and **Judith Frydman**[3]

1*Graduate Program in Structural and Computational Biology and Molecular Biophysics, Verna and Marrs McLean Department of Biochemistry and Molecular Biology, One Baylor Plaza, Baylor College of Medicine, Houston, Texas 77030, USA*

2*National Center for Macromolecular Imaging, Verna and Marrs McLean Department of Biochemistry and Molecular Biology, One Baylor Plaza, Baylor College of Medicine, Houston, Texas 77030, USA*

3*Department of Biological Sciences and BioX Program, Clark Center E200A, Stanford University, Stanford, California 94305−5020, USA*

4*Departments of Biopharmaceutical Sciences and Pharmaceutical Chemistry and California Institute for Quantitative Biomedical Research, University of California at San Francisco, 1700 4th Street, San Francisco, California 94158−2330, USA*

## Abstract

All chaperonins mediate ATP-dependent polypeptide folding by confining substrates within a central chamber. Intriguingly, the eukaryotic chaperonin TRiC (also called CCT) uses a built-in lid to close the chamber, whereas prokaryotic chaperonins use a detachable lid. Here we determine the mechanism of lid closure in TRiC using single-particle cryo-EM and comparative protein modeling. Comparison of TRiC in its open, nucleotide-free, and closed, nucleotide-induced states reveals that the interdomain motions leading to lid closure in TRiC are radically different from those of prokaryotic chaperonins, despite their overall structural similarity. We propose that domain movements in TRiC are coordinated through unique interdomain contacts within each subunit and, further, these contacts are absent in prokaryotic chaperonins. Our findings show how different mechanical switches can evolve from a common structural framework through modification of allosteric networks.

The folding of newly made polypeptides to their native conformation is one of the least understood steps in the expression of genetic information. Defects in this process are associated with various pathological states, including cancer and amyloid diseases[1,2]. Molecular chaperones have an essential role in mediating cellular protein folding and facilitating the misfolded proteins[3,4]. Accordingly, these large, ATP-dependent chaperone assemblies are widely conserved throughout all kingdoms of life[3,4].

The large ring-shaped chaperonins are among the most structurally complex and mechanistically intriguing cytosolic chaperones[5,6]. Chaperonins consist of two stacked

multisubunit rings, each with a large inner chamber that accommodates the folding polypeptide[5,6]. Folding is thought to occur within the central chamber upon ATP-dependent encapsulation of the bound substrate. Although the overall architecture of chaperonins is highly conserved, two structurally and mechanistically distinct types of chaperonins have emerged throughout evolution. Importantly, these two classes of chaperonin, the so-called Group I and Group II chaperonins, differ radically in their substrate-folding abilities, and substrates for one class of chaperonin cannot generally be folded by the other[7–9].

Group I chaperonins, such as the well-characterized GroEL from *Escherichia coli*, are found in prokaryotes and organelles of endosymbiotic origin. GroEL is composed of 14 identical subunits arranged in two stacked, seven-membered rings. Lid closure is achieved upon ATP-dependent binding of a seven-membered ring cofactor, GroES, which acts as a detachable lid that encapsulates the polypeptide substrate within the central cavity[10]. GroES binding leads to dramatic GroEL rearrangements that release the bound polypeptides, allowing them to fold within the protected environment of the cavity[11–13].

The Group II chaperonins, found in eukaryotes and archaea, share the same overall architecture, yet are substantially different from bacterial chaperonins[5,6]. Unlike GroEL, most Group II chaperonins are hetero-oligomeric. For instance, the chaperonin TRiC (for TCP-1 ring complex, also called CCT), consists of eight different paralogous subunits per ring[6,14]. Importantly, Group II chaperonins lack a GroES-type cofactor acting as a detachable lid. Instead, lid formation involves the transformation of flexible protrusions inserted at the tip of the apical domains into a β-stranded iris that acts as a lid over the central cavity[15–17]. The built-in lid of Group II chaperonins shares some of the functions of GroES on GroEL[13], such as regulation of allostery within the chaperonin subunits and encapsulation of the polypeptide substrate upon lid closure[12,17–20]. Furthermore, lidless chaperonins lose the ability to fold stringent substrates[17,19,21], suggesting that the apical protrusions indeed fulfill a GroES-like function in Group II chaperonins. However, whereas GroES binding to GroEL occurs upon ATP binding, formation of the built-in lid in eukaryotic and archaeal chaperonins is triggered by the transition state of ATP hydrolysis, indicating mechanistic differences in how the nucleotide cycle drives lid closure[17]. Additionally, lid closure has been proposed to follow a sequential allosteric mechanism rather than the concerted manner observed for Group I chaperonins[22]. The distinct mechanism of lid closure of the eukaryotic chaperonins probably contributes to its functional differences from bacterial chaperonins, such as its co-translational interaction with substrates and unique ability to fold eukaryotic proteins, such as actin, that cannot be folded by prokaryotic chaperonins[7,9].

Given their centrality for cellular protein folding, chaperonin's mechanisms have been the focus of intense study. Intriguingly, crystallographic analysis of bacterial and archaeal chaperonins revealed that the domain structure and backbone traces of Group I and Group II chaperonin subunits are highly conserved[23–26]. In both Group I and Group II chaperonins, each subunit consists of three domains connected by flexible linkers. The equatorial domain is the site of nucleotide binding and provides the inter-ring contacts, the apical domain contains the substrate binding site and the intermediate or hinge domain connects the equatorial and apical domains. Whereas the Group I apical domains contain a GroES binding site, the Group II apical domains contain a flexible loop insertion that forms the lid upon closure.

The striking structural similarity between Group I and Group II chaperonins raises the question of how they can support such different mechanisms of lid closure. Addressing this question would require comparing the movements leading to lid closure in Group I and Group II chaperonins. Unfortunately, this has been hindered by our limited understanding of how the lid closes in Group II chaperonins. The conformational rearrangements leading to lid closure in Group II chaperonins remain unclear. Current models of lid closure in Group II chaperonins

stemming from low-resolution cryo-EM analyses of TRiC[27–29] propose that ATP binding would bring down the protrusions to close the lid, but would otherwise produce minimal twisting of the apical domains[14,27]. This would be a radical departure from lid closure for GroEL, which is accompanied by large rotational domain motions induced by ATP and GroES binding[30]. However, the low resolution of the TRiC cryo-EM maps was not sufficient to allow for analysis of domain positioning[28,29], and thus they do not provide any structural insight into how the conserved chaperonin subunit architecture could lead to such different molecular motions.

Here we address the question of how the highly conserved chaperonin architecture can support such dramatically different mechanisms of lid closure: a detachable lid in bacteria and a built-in lid in eukaryotes. To this end, we combined single-particle cryo-EM with comparative protein structure modeling to derive detailed pseudo atomic models of bovine TRiC with its lid in the open and closed states. Our data identifies the molecular motions that accompany lid closure in the eukaryotic chaperonin TRiC. We find that, unlike what was previously proposed, the ATP-induced movements leading to lid closure change the properties of the central chamber facing the substrate, with important implications for TRiC function. Notably, our data reveal that the conformational change in the chaperonin ATPase domain is conserved across chaperonins but drives a different motion in the TRiC apical domains from that it produces in GroEL, by virtue of a remodeled interface between the apical and intermediate domain. Thus, our pseudo atomic models provide a structural rationale for the crucial differences between the motions accompanying lid closure in TRiC and GroEL, suggesting how the same chaperonin architecture can support two radically different mechanisms of closure through remodeling its allosteric networks.

# RESULTS

## Visualizing the open and closed conformations of TRiC

To obtain functionally relevant structural information, we prepared folding-active chaperonin samples with their lids in either the open conformation or in a stable, symmetrically closed state under previously characterized conditions that maintain chaperonin activity (Methods and Supplementary Fig. 1 online)[17]. We examined these chaperonin states by cryo-EM and single-particle analysis techniques to generate three-dimensional reconstructions of TRiC in the open and the closed conformations (Fig. 1a–c for the closed state and Fig. 1d–f for the open state). Both reconstructions made the assumption that the TRiC structures have eight-fold symmetry, on the basis of the symmetry of similar archaebacterial chaperonins and the high sequence conservation between archaeal and eukaryotic chaperonin subunits[25,31]. The structure of the closed ATP-induced TRiC state, assessed at 15-Å resolution using the 0.5 Fourier Shell Correlation (FSC) criterion, was notably similar to the X-ray structures of related archaeal chaperonins (for example, PDB 1A6D and 1A6E[25]). Indeed, the cryo-EM density map for the symmetrically closed TRiC state was almost indistinguishable from the closed archaeal crystal structure blurred out to a comparable resolution to the cryo-EM reconstruction (Supplementary Fig. 2 online).

The TRiC open conformation, obtained in the absence of nucleotide, was assessed at 18-Å resolution using the 0.5 FSC criterion. TRiC in the open state was more elongated than in the closed state and showed a dramatic expansion of the central cavity. Notably, the more elongated TRiC shape in the open state was consistent with previous small-angle X-ray scattering (SAXS) solution measurements of TRiC, indicating that the EM maps reflect the solution structure of the complex. Comparison of these TRiC three-dimensional reconstructions revealed that ATP-induced lid closure results in dramatic differences in the conformations of this protein-folding nanomachine (Fig. 1).

## Pseudo atomic models of open and closed conformations

The reconstructions for the two conformational states of TRiC obtained above were sufficiently resolved to identify confidently the different domains of the individual three-domain subunits. Accordingly, we sought to gain insight into the molecular motions leading to lid closure by deriving pseudo atomic models of TRiC in the open and closed state from the EM-derived three-dimensional density maps.

To build homology-based protein structure models for individual TRiC subunits in the closed state, we exploited the observation that the closed conformation of TRiC was strikingly similar to the high-resolution structures of the related archaeal chaperonins, with which they share a high level of sequence conservation (35−41% sequence identity; Fig. 2a for subunit α, and Supplementary Figs. 3 and 4 online)[31,32]. Indeed, the models we generated for the closed TRiC subunits fit well into the density of a single subunit segmented from the cryo-EM density map (Fig. 2b). We then assembled a pseudo atomic model for the entire TRiC ring in the closed state using a previously proposed intra-ring subunit arrangement[33] (Fig. 2c,d).

We next derived a model of TRiC in its open conformation (Fig. 3). The absence of crystallographic information about the open conformation of either TRiC or any other archaeal Group II chaperonins precludes straightforward homology modeling of the TRiC subunits in the open state. However, the overall architecture and individual domain structure of eukaryotic and prokaryotic chaperonins are strikingly similar[5,15,34,35]. Furthermore, both use ATP as an allosteric effector to drive lid closure[6,13]. Therefore, we derived the model for the open state of TRiC using the assumption that, similarly to what happens in GroEL, the nucleotide-induced conformational change in Group II chaperonin subunits also involves rigid body motions of each domain around flexible hinges[12,13] (Methods). Indeed, the known hinge regions driving the conformational change in Group I chaperonins are also conserved in each TRiC subunit. In further support of this assumption, these same regions were also independently identified as flexible hinges in both the archaeal subunits and the TRiC homology models using normal mode analysis[36–41] (Methods). The domains of TRiC, each separated by hinge regions, were docked into the TRiC open-conformation reconstruction and then used as a template for refinement through homology modeling and energy minimization to obtain a refined open-state model for the TRiC subunits.

The open-state model for each subunit (Fig. 3a) fits well into the density of a single subunit segmented from the cryo-EM map (Fig. 3b). Notably, the only region in the model that did not fit the cryo-EM map was the short segment that forms the lid in the closed state, suggesting that this region may be too flexible in the open conformation to be observed by cryo-EM. Indeed, previous biochemical and biophysical analyses indicate that the lid segments are highly dynamic in the open TRiC state[17,42]. Together, these data indicate that this region is unstructured in the open state, whereas it is structured in the closed state observed in the crystals used to derive the model. Thus, the lack of cryo-EM density for the lid regions in the open state is entirely consistent with their biochemical properties and the solution conformation of this structure, and validates the biological relevance of the open TRiC structure.

## An iris-like conformational change drives lid closure in TRiC

The models obtained for TRiC in the open (Fig. 3c,d) and closed (Fig. 2c,d) states provide end points from which to derive the ATP-induced molecular motions leading to lid closure (Fig. 3e). Comparing these conformations suggests that lid formation results from ATP-induced movements of the intermediate and apical domains, whereas the equatorial domains are relatively stationary (Fig. 4a,b and Supplementary Video 1 online). Within the assumption of eight-fold symmetry, these movements, viewed in the context of the entire ring, reveal that TRiC uses a concerted lateral rotation motion of apical and intermediate domains to form the

lid and close off access to the central cavity (Supplementary Videos 1 and 2 online). These motions are consistent with our results from the low-frequency motion in a normal mode analysis[36–38,40,41] (NMA; Supplementary Videos 3 and 4 online).

We next used our analysis to gain a molecular understanding of how the conserved chaperonin structure leads to radically different strategies to convert ATP-induced changes into closure of the central chamber. Comparing our models of TRiC in the open and closed states to the crystal structures of GroEL in the open and the closed, GroES-bound states provides intriguing clues as to the molecular features underlying their distinct mechanisms of lid closure (Fig. 4). Notably, ATP induces similar movements in the intermediate domains of GroEL and TRiC, bringing together residues of both the equatorial and intermediate domains to form a tight pocket that mediates nucleotide hydrolysis[25]. This observation is consistent with the high degree of conservation of these residues at the interface of the intermediate and equatorial domains of bacterial and eukaryotic chaperonins[25,30]. However, this conserved ATP-induced change leads to dramatically different motions in the apical domains of TRiC and GroEL (Fig. 4). Whereas the TRiC apical domains rotate in the same direction as the intermediate domain to close the lid (around the relative positions of stars in Fig. 4a,b and Supplementary Video 1), the GroEL apical domains rotate in the opposite direction from the intermediate domain, tilting upwards and away from the cavity to bind GroES (relative positions of stars in Fig. 4c,d)[30]. As discussed below (Fig. 5), this striking difference arises from the distinct nature of the interdomain interfaces connecting the apical and intermediate domains.

An important corollary of our structural analysis is that the nucleotide-induced change in equatorial and intermediate domains is largely conserved between Group I and Group II chaperonins, but that this conserved conformational change is transmitted differently throughout the chaperonin subunits, resulting in dramatic differences in the movements of the apical domains and, consequently, a radically different mechanism of lid closure. As discussed below, we propose that these different mechanisms are supported by the remodeling of the allosteric network in Group II chaperonins.

## DISCUSSION

The eukaryotic chaperonin TRiC facilitates the folding of a wide spectrum of cytosolic proteins, including many essential structural and regulatory proteins such as actin, tubulin and several signal transduction and cell-cycle regulators[6]. Notably, many of its substrates cannot be folded by any other chaperone in the cell, suggesting that TRiC has acquired unique features that distinguish it from other chaperones[7,9]. The understanding of the molecular motions leading to lid closure in TRiC obtained in this study has important implications for the strategies used to fold its cellular substrates. Additionally, the molecular models derived for the open and closed conformations of TRiC reveal how the evolutionary restructuring of the chaperonin allosteric network allowed the conserved chaperonin architecture to support the unique lid structure found in eukaryotic chaperonins.

### Implications of lid closure mechanism for the folding reaction

Our data suggest that in the eukaryotic chaperonin TRiC the built-in lid involves the nucleotide-induced lateral twisting of the apical and intermediate domains (Supplementary Videos 1 and 2). This finding has important implications for our understanding of how TRiC promotes substrate folding. Previous models proposed that lid closure occurred without domain rotation. Accordingly, the properties of the central chamber would remain largely unchanged upon lid closure, with the same substrate binding sites accessible in the open state still exposed to the cavity in the closed state[14]. Because the substrate binding sites would contact the substrate in both open and closed states, this model raised the question of how the substrate would be released during the ATPase cycle. In contrast, our structures indicate that lid closure involves

an ATP-induced rotation of the apical domains. Because the nature of the central chamber facing the substrate will be different in the open and closed states, our analysis suggests that lid closure will substantially alter the folding environment in the chaperonin cavity. The idea that the residues facing the cavity change between the open and closed states has important implications for the TRiC-mediated folding reaction. First, by changing the chemical environment facing the substrate upon lid closure, Group II chaperonins could use confinement to promote folding, as observed in Group I chaperonins[11]. Second, our data propose a model of how release of the native substrates can be achieved upon ATP-induced folding.

The structural transition proposed by our work also explains several biochemical observations that are inconsistent with the idea that the interior cavity is lined by the same polar surfaces in the open and closed states[43,44]. Thus, biochemical experiments from several laboratories indicated that TRiC in its open state binds substrates through hydrophobic interactions[45–47], whereas no obvious hydrophobic surfaces are exposed to the cavity in closed models of TRiC. Additionally, a recent study mapped the substrate binding sites of TRiC to an apical domain location similar to that of the GroEL binding sites, which would not be exposed to the cavity in the former model[48]. Importantly, these biochemical observations are in agreement with the mechanism that emerges from our structural studies, in which the binding sites exposed in the open state differ from the surface that faces the substrate in the closed state. Of note, the nature of the putative substrate binding sites in the apical domains of TRiC[48] is not invariably hydrophobic in all the different subunits in the ring, but instead varies depending on the TRiC subunit, with some binding sites having a more hydrophobic character and others being lined with polar residues[16]. Accordingly, our model suggests that a substrate may bind combinatorially to several distinct binding sites in the apical domains of an open molecule of TRiC, perhaps combining polar and hydrophobic interactions. If this is the case, the closing of the lid would create a chamber that has new chemical properties that presumably create a nanocage optimized to promote the folding of eukaryotic substrates of TRiC.

Because our cryo-EM reconstructions are based on the assumption of eight-fold symmetry within each ring, as are all current reconstructions of TRiC, our proposed model is probably a simplification of the actual mechanism of lid formation. For instance, a recent study proposed that ATP-induced conformational changes in TRiC spread around the ring in a sequential fashion, in contrast to what is observed for Group I chaperonins[22]. As the lid has an important role coordinating intra-ring allostery[19], it is likely that the unique mode of lid closure facilitated the emergence of the sequential allosteric mechanism observed in Group II chaperonins.

One potentially exciting avenue of investigation for the future is to remove the assumption of symmetry in the reconstruction process, which will require at least eight times as many particle images and 100 times more computational power to accomplish. Such effort will inevitably be required to unravel the complexity of this structurally dynamic protein-folding machinery and to pinpoint the exact location of the substrate binding sites within the complex.

## Remodeling the allosteric networks in homologous chaperonins

Our results provide, for the first time, insight into how the similar chaperonin architectures of TRiC and GroEL can support their divergent mechanisms of lid closure. The structural models for the two conformations of TRiC obtained here reveal both similarities and differences between the molecular motions of TRiC and its prokaryotic homolog GroEL. Interestingly, both similarities and differences illuminate how evolution shaped these distinct lid-closing mechanisms. We find that the movements induced by ATP in the nucleotide binding pockets are similar among Group I and Group II chaperonins, consistent with the high conservation in the nucleotide binding pocket. In contrast, the conserved conformational change is transmitted differently, as the apical domains of TRiC and GroEL rotate in opposite directions during lid closure. This difference in molecular motions led us to compare the apical intermediate domain

interfaces in the X-ray structures of GroEL with those in the structures of the TRiC-like archaeal chaperonin[25] (Fig. 5). Notably, whereas the archaeal chaperonins contain three and four putative hydrogen bonds bridging the apical and intermediate domains in the α and β subunits, respectively (Fig. 5a, shown for the α subunit), no hydrogen or electrostatic bonds are observed linking the apical and intermediate domains of a single subunit in either the apo or liganded GroEL structures (Fig. 5b,c). Additionally, the buried surface area between the apical and intermediate domains of archaeal chaperonin subunits is substantially larger than that for GroEL subunits in either conformation (1,480$\text{Å}^2$ for the α-thermosome compared to 380$\text{Å}^2$ and 430$\text{Å}^2$ for GroEL in the closed and open states, respectively). Thus, despite the great structural similarity of the two chaperonins and the fact that the hinges between the domains of each molecule are in approximately the same location, we find that the interface between the apical and intermediate domains is radically remodeled in Group II chaperonins. Notably, the homology models for all TRiC subunits also predict a substantial buried area and the formation of one to four hydrogen bonds between their apical and intermediate domains (data not shown). Our analysis suggests that additional contacts stabilize the interface between the apical and intermediate domains in the subunits of eukaryotic and archaeal chaperonins. The presence of these additional interdomain contacts provides a plausible structural rationale for our observation that the apical and intermediate domains of TRiC rotate together in the same direction upon nucleotide hydrolysis, allowing the closure of the built-in lid.

The implications of our cryo-EM–based analysis of TRiC reach beyond an understanding of chaperonin mechanism, as our work provides insights into the evolution of protein machines. Despite the architectural similarity between TRiC and GroEL, they seem to have acquired their distinct mechanisms of action through the evolution of a select set of interdomain contacts that determine how the ATP-induced allosteric signal is transmitted throughout the protein subunit. Our analysis reveals how two protein machines with high overall structural similarity can function through dramatically different molecular movements and mechanisms, by incorporating subtle changes into their allosteric networks. A better understanding of the principles that establish these alternate allosteric networks may eventually be exploited to engineer chaperonins with different functionalities.

## METHODS

### TRiC purification and specimen preparation

We purified TRiC from bovine testes essentially as described[49], but incorporated an ultracentrifugation step through 20−60% (w/v) sucrose cushions before chromatographic purification. Copurifying bound substrates were removed from TRiC by incubation with ATP before chromatography. Most TRiC particles in our preparation were active, based on the stoichiometry of actin binding, the efficiency of actin binding (60−80% folding after 45 min at 30 °C) and the efficiency of conversion to the closed state in the presence of ATP and AlF$_x$ (~100% as assayed by proteolytic digestion; see also ref. [17] and Supplementary Fig. 1).

TRiC samples were prepared for cryo-EM studies by dilution of purified TRiC to 1 mg ml$^{-1}$ in buffer A (20 mM HEPES-KOH, pH 7.4, 100 mM potassium acetate, 5 mM magnesium acetate). Nucleotide-free samples were used immediately, whereas ATP-AlF$_x$ samples were incubated in the presence of 1 mM ATP (Sigma), 5 mM Al(NO$_3$)$_3$, and 30 mM NaF for 1 h at 30 °C before being frozen.

Samples were embedded in vitreous ice as follows. We placed a 3 μl aliquot of TRiC sample onto a washed, glow-discharged, 200-mesh R2−1 Quantifoil continuous carbon grid (Quantifoil Micro Tools GmbH, Jena, Germany). The grid was blotted and flash frozen in liquid ethane using a Vitrobot (FEI). We stored the grids in liquid nitrogen until they were imaged.

### Image collection

We acquired ice-embedded images at an effective magnification of 83,100× on a US4000 charge-coupled device (CCD) camera (Gatan Inc.) using a JEOL2010F electron microscope (JEOL Inc.) with a field emission gun operated at 200 kV. A custom software package, JAMES[50], was used to acquire focal pairs of images semiautomatically, at a range of 0.8−2.5 µm underfocus for the first image and a range of 2−5 µm underfocus for the second image.

### Image preprocessing

An initial three-dimensional model was created using the EMAN program startcsym (http://ncmi.bcm.tmc.edu/software/)[51] by manually selecting all the particles in a few representative micrographs. We genereated references from the initial model and used them to select the particles from the far-from-focus CCD frames using the automatic reference-based particle selection method in the EMAN software program batchboxer[51]. The far-from-focus boxes were aligned to their close-to-focus counterparts using the EMAN program boxer[51]. The automatically selected particles were visually screened using the EMAN program boxer[51] such that every nonover-lapping TRiC particle was selected. Contrast transfer function (CTF) parameters were initially estimated using the EMAN program ctfit[51]. Final CTF parameters were determined by manually fitting a theoretical one-dimensional power spectrum to a one-dimensional power spectrum calculated from the boxed particles for each micrograph using the EMAN program ctfit[51]. Using these procedures, 7,129 particles of ATP-AlF$_x$ TRiC and 13,287 particles of nucleotide-free TRiC were prepared for the three-dimensional reconstruction.

### Three-dimensional reconstruction

We carried out particle orientations and three-dimensional reconstruction as described previously[52,53]. Briefly, the entire data set of raw particles was subjected to a multirefine-based procedure as described previously[52], using two starting models created using the EMAN program startcsym[51] that had different amounts of applied noise. After this step, the class with the most particles assigned to it was further refined using the standard EMAN iterative reconstruction algorithm[53]. Briefly, the iterative reconstruction consists of reference-based classification of particles, class-averaging with CTF correction and three-dimensional model construction. The iterative reconstruction process continued until convergence was achieved, as assessed by observing the iteration-to-iteration Fourier shell correlation (FSC) curve. We made no reference to previously determined structural information during the reconstruction process; the only assumption made was an imposition of C8 symmetry. The density maps were scaled for visualization so that an isosurface threshold of 1 would correspond to the approximate molecular weight of the TRiC complex. Resolution of the reconstruction was estimated using the 0.5 FSC criterion between two reconstructions generated from even- and odd-numbered particles, respectively. All visualization was done with the UCSF Chimera molecular visualization package (http://www.cgl.ucsf.edu/chimera/)[54] or the PyMOL Molecular Graphics System (http://www.pymol.org/).

### Comparative modeling of TRiC closed (complexed with ATP-AlFx) state

We carried out homology or comparative protein-structure modeling using the program MODELLER[32]. Each of the eight bovine TRiC subunits (TIGR: TCPA_BOS, TCPB_BOS, TCPD_BOS, TCPE_BOS, TCPG_BOS, TCPH_BOS, TCPQ_BOS, TCPZ_BOS) was modeled using the standard multiple-template modeling protocol implemented in the 'model' module. For the TRiC closed state, the thermosome structure from *Thermoplasma acidophilum* (PDB 1A6E) and the N and C termini from the thermosome structure found in *Thermococcus* strain KS-1 (PDB 1Q3Q) were used as templates. Both templates have a sequence identity to the bovine sequences ranging from 35% to 41%. For each of the subunits,

50 models were generated by MODELLER, and the best one was selected by the multivariate model assessment score[55]. Inaddition, for loop regions with relatively low sequence similarity to the templates, 200 models for each of those loop regions were generated by the 'loop' module, and the best one was chosen by the DOPE statistical potential score[55], in combination with the higher docking score to the cryo-EM density map[56] obtained by the EMAN program foldhunter[57]. We built a complete model of the eight-subunit ring using the subunit permutation previously proposed[33].

Finally, we subjected this complete model to another round of MODELLER refinement to improve its stereochemistry. The refined model of the eight-subunit structure was docked into the TRiC-closed cryo-EM map using the rigid body docking program from EMAN, foldhunter[57], with the similarity score of 0.987 calculated by the EMAN program fh-stat.py. Although each subunit in the model was well docked within the density map, at this level of resolution, a similarly good fit would be obtained with a different subunit arrangement.

### TRiC open-state comparative modeling and domain docking

The thermosome structure from *T. acidophilum* (PDB 1A6D) and the N and C termini of the thermosome from the *Thermococcus* strain KS-1 (PDB 1Q3R) were chosen as templates. These PDB structures were used because they corresponded to the nucleotide-free state. Both of the templates have a sequence identity ranging from 35% to 41% to the bovine sequences. We carried out modeling of each of the subunits as described above. The best model of each subunit was docked into the cryo-EM density of the TRiC open state according to the proposed subunit arrangement[33]. This initial docking was refined by breaking the subunit into three domains (Fig. 3a). Domain boundaries were initially assigned analogously to those in the thermosome[25] and GroEL[30] and verified through normal mode analysis of the comparative models[39] using the Molecular Modeling Toolkit (http://dirac.cnrs-orleans.fr/MMTK/).

We performed the docking of each of the three domains to the TRiC open-state cryo-EM map independently, resulting in a similarity score of 0.963, 0.980 and 0.971 for the α subunit apical, intermediate and equatorial domains, respectively, as assessed by the EMAN program fh-stat.py[57]. These three rigid-body docked domains were then used together as a template, for a new round of model generation with MODELLER, to refine the structure and reestablish the broken chemical bonds in the hinge regions between the domains. Finally, we applied the same loop refinement and quaternary model building procedures described above. The optimized eight-subunit comparative model was docked into the TRiC open-state density map using foldhunter[57], resulting in the similarity score of 0.969 as evaluated by the EMAN program fh-stat.py.

### Comparing comparative models for the open and closed states

The trajectory of transition between the two docked conformations was modeled by linear interpolation between these two states using the morph.tcl script in the VMD software package (http://www.ks.uiuc.edu/Research/vmd/). The buried surface area between the apical and intermediate domains of GroEL and the thermosome was calculated using the g_sas module from GROMACS (http://www.gromacs.org/)[58].

### Normal mode analysis on the TRiC open (nucleotide-free) state

We carried out NMA[36–38,40,41] on the comparative model of the apo TRiC (open state) to investigate the motions of TRiC in its native state. The same procedure was adopted as described previously[37]. Low-frequency modes from NMA represent large global conformational changes observed in biological systems[41]. The lowest-frequency nondegenerate normal mode, mode 1, is shown in Supplementary Videos 3 and 4, in which only Cα atoms were illustrated in the space-filling style. The top view of mode 1

(Supplementary Video 3) clearly shows a rotation motion of the apical domains around the eight-fold rotational axis. Meanwhile, the side view of this mode (Supplementary Video 4) shows that the intermediate domains rotate together with the apical domains in the same direction, whereas the equatorial domains maintain their original position. The motions interpreted from mode 1, the lowest-frequency nondegenerate normal mode, are highly consistent with the mechanism of lid closure proposed in this study on the basis of our open and closed TRiC cryo-EM reconstructions and corresponding homology models.

## ACKNOWLEDGMENTS

## References

1. Dobson CM. Principles of protein folding, misfolding and aggregation. Semin. Cell Dev. Biol 2004;15:3–16. [PubMed: 15036202]

2. Gregersen N, Bross P, Jorgensen MM, Corydon TJ, Andresen BS. Defective folding and rapid degradation of mutant proteins is a common disease mechanism in genetic disorders. J. Inherit. Metab. Dis 2000;23:441–447. [PubMed: 10947197]

3. Frydman J. Folding of newly translated proteins *in vivo*: the role of molecular chaperones. Annu. Rev. Biochem 2001;70:603–647. [PubMed: 11395418]

4. Hartl FU, Hayer-Hartl M. Molecular chaperones in the cytosol: from nascent chain to folded protein. Science 2002;295:1852–1858. [PubMed: 11884745]

5. Sigler PB, et al. Structure and function in GroEL-mediated protein folding. Annu. Rev. Biochem 1998;67:581–608. [PubMed: 9759498]

6. Spiess C, Meyer AS, Reissmann S, Frydman J. Mechanism of the eukaryotic chaperonin: protein folding in the chamber of secrets. Trends Cell Biol 2004;14:598–604. [PubMed: 15519848]

7. Frydman J, et al. Function in protein folding of TRiC, a cytosolic ring complex containing TCP-1 and structurally related subunits. EMBO J 1992;11:4767–4778. [PubMed: 1361170]

8. Kerner MJ, et al. Proteome-wide analysis of chaperonin-dependent protein folding in *Escherichia coli*. Cell 2005;122:209–220. [PubMed: 16051146]

9. Tian G, Vainberg IE, Tap WD, Lewis SA, Cowan NJ. Specificity in chaperonin-mediated protein folding. Nature 1995;375:250–253. [PubMed: 7746329]

10. Fenton WA, Horwich AL. Chaperonin-mediated protein folding: fate of substrate polypeptide. Q. Rev. Biophys 2003;36:229–256. [PubMed: 14686103]

11. Brinker A, et al. Dual function of protein confinement in chaperonin-assisted protein folding. Cell 2001;107:223–233. [PubMed: 11672529]

12. Bukau B, Horwich AL. The Hsp70 and Hsp60 chaperone machines. Cell 1998;92:351–366. [PubMed: 9476895]

13. Saibil HR, Ranson NA. The chaperonin folding machine. Trends Biochem. Sci 2002;27:627–632. [PubMed: 12468232]

14. Valpuesta JM, Martin-Benito J, Gomez-Puertas P, Carrascosa JL, Willison KR. Structure and function of a protein folding machine: the eukaryotic cytosolic chaperonin CCT. FEBS Lett 2002;529:11–16. [PubMed: 12354605]

15. Gutsche I, Essen LO, Baumeister W. Group II chaperonins: new TRiC(k)s and turns of a protein folding machine. J. Mol. Biol 1999;293:295–312. [PubMed: 10550210]

16. Leroux MR, Hartl FU. Protein folding: versatility of the cytosolic chaperonin TRiC/CCT. Curr. Biol 2000;10:R260–R264. [PubMed: 10753735]

17. Meyer AS, et al. Closing the folding chamber of the eukaryotic chaperonin requires the transition state of ATP hydrolysis. Cell 2003;113:369–381. [PubMed: 12732144]

18. Kafri G, Willison KR, Horovitz A. Nested allosteric interactions in the cytoplasmic chaperonin containing TCP-1. Protein Sci 2001;10:445–449. [PubMed: 11266630]

19. Reissmann S, Parnot C, Booth CR, Chiu W, Frydman J. Essential function of the built-in lid in the allosteric regulation of eukaryotic and archaeal chaperonins. Nat. Struct. Mol. Biol 2007;14:432–440. [PubMed: 17460696]

20. Yoshida T, et al. Archaeal group II chaperonin mediates protein folding in the *cis*-cavity without a detachable GroES-like co-chaperonin. J. Mol. Biol 2002;315:73–85. [PubMed: 11771967]

21. Iizuka R, et al. Role of the helical protrusion in the conformational change and molecular chaperone activity of the archaeal group II chaperonin. J. Biol. Chem 2004;279:18834–18839. [PubMed: 14978026]

22. Rivenzon-Segal D, Wolf SG, Shimon L, Willison KR, Horovitz A. Sequential ATP-induced allosteric transitions of the cytoplasmic chaperonin containing TCP-1 revealed by EM analysis. Nat. Struct. Mol. Biol 2005;12:233–237. [PubMed: 15696173]

23. Boisvert DC, Wang J, Otwinowski Z, Horwich AL, Sigler PB. The 2.4 crystal structure of the bacterial chaperonin GroEL complexed with ATPγS. Nat. Struct. Biol 1996;3:170–177. [PubMed: 8564544]

24. Braig K, et al. The crystal structure of the bacterial chaperonin GroEL at 2.8. Nature 1994;371:578–586. [PubMed: 7935790]

25. Ditzel L, et al. Crystal structure of the thermosome, the archaeal chaperonin and homolog of CCT. Cell 1998;93:125–138. [PubMed: 9546398]

26. Shomura Y, et al. Crystal structures of the group II chaperonin from *Thermococcus* strain KS-1: steric hindrance by the substituted amino acid, and inter-subunit rearrangement between two crystal forms. J. Mol. Biol 2004;335:1265–1278. [PubMed: 14729342]

27. Llorca O, et al. The 'sequential allosteric ring' mechanism in the eukaryotic chaperonin-assisted folding of actin and tubulin. EMBO J 2001;20:4065–4075. [PubMed: 11483510]

28. Llorca O, et al. Eukaryotic chaperonin CCT stabilizes actin and tubulin folding intermediates in open quasi-native conformations. EMBO J 2000;19:5971–5979. [PubMed: 11080144]

29. Llorca O, et al. Eukaryotic type II chaperonin CCT interacts with actin through specific subunits. Nature 1999;402:693–696. [PubMed: 10604479]

30. Xu Z, Horwich AL, Sigler PB. The crystal structure of the asymmetric GroELGroES-(ADP)7 chaperonin complex. Nature 1997;388:741–750. [PubMed: 9285585]

31. Kubota H, Hynes G, Carne A, Ashworth A, Willison K. Identification of six Tcp-1-related genes encoding divergent subunits of the TCP-1-containing chaperonin. Curr. Biol 1994;4:89–99. [PubMed: 7953530]

32. Sali A, Blundell TL. Comparative protein modelling by satisfaction of spatial restraints. J. Mol. Biol 1993;234:779–815. [PubMed: 8254673]

33. Liou AK, Willison KR. Elucidation of the subunit orientation in CCT (chaperonin containing TCP1) from the subunit composition of CCT micro-complexes. EMBO J 1997;16:4311–4316. [PubMed: 9250675]

34. Saibil H. Molecular chaperones: containers and surfaces for folding, stabilising or unfolding proteins. Curr. Opin. Struct. Biol 2000;10:251–258. [PubMed: 10753820]

35. Young JC, Agashe VR, Siegers K, Hartl FU. Pathways of chaperone-mediated protein folding in the cytosol. Nat. Rev. Mol. Cell Biol 2004;5:781–791. [PubMed: 15459659]

36. Brooks B, Karplus M. Harmonic dynamics of proteins: normal modes and fluctuations in bovine pancreatic trypsin inhibitor. Proc. Natl. Acad. Sci. USA 1983;80:6571–6575. [PubMed: 6579545]

37. Chacon P, Tama F, Wriggers W. Mega-Dalton biomolecular motion captured from electron microscopy reconstructions. J. Mol. Biol 2003;326:485–492. [PubMed: 12559916]

38. Go N, Noguti T, Nishikawa T. Dynamics of a small globular protein in terms of low-frequency vibrational modes. Proc. Natl. Acad. Sci. USA 1983;80:3696–3700. [PubMed: 6574507]

39. Hinsen K. The molecular modeling toolkit: a new approach to molecular simulations. J. Comput. Chem 2000;21:79–85.

40. Ma J, Karplus M. The allosteric mechanism of the chaperonin GroEL: a dynamic analysis. Proc. Natl. Acad. Sci. USA 1998;95:8502–8507. [PubMed: 9671707]

41. Tama F, Brooks CL, III. Diversity and identity of mechanical properties of icosahedral viral capsids studied with elastic network normal mode analysis. J. Mol. Biol 2005;345:299–314. [PubMed: 15571723]

42. Heller M, et al. NMR studies on the substrate-binding domains of the thermosome: structural plasticity in the protrusion region. J. Mol. Biol 2004;336:717–729. [PubMed: 15095983]

43. Gomez-Puertas P, Martin-Benito J, Carrascosa JL, Willison KR, Valpuesta JM. The substrate recognition mechanisms in chaperonins. J. Mol. Recognit 2004;17:85–94. [PubMed: 15027029]

44. Pappenberger G, et al. Crystal structure of the CCTγ apical domain: implications for substrate binding to the eukaryotic cytosolic chaperonin. J. Mol. Biol 2002;318:1367–1379. [PubMed: 12083524]

45. Feldman DE, Spiess C, Howard DE, Frydman J. Tumorigenic mutations in VHL disrupt folding *in vivo* by interfering with chaperonin binding. Mol. Cell 2003;12:1213–1224. [PubMed: 14636579]

46. Kubota S, Kubota H, Nagata K. Cytosolic chaperonin protects folding intermediates of Gβ from aggregation by recognizing hydrophobic β-strands. Proc. Natl. Acad. Sci. USA 2006;103:8360–8365. [PubMed: 16717193]

47. Rommelaere H, De Neve M, Melki R, Vandekerckhove J, Ampe C. The cytosolic class II chaperonin CCT recognizes delineated hydrophobic sequences in its target proteins. Biochemistry 1999;38:3246–3257. [PubMed: 10079067]

48. Spiess C, Miller EJ, McClellan AJ, Frydman J. Identification of the TRiC/CCT substrate binding sites uncovers the function of subunit diversity in eukaryotic chaperonins. Mol. Cell 2006;24:25–37. [PubMed: 17018290]

49. Ferreyra RG, Frydman J. Purification of the cytosolic chaperonin TRiC from bovine testis. Methods Mol. Biol 2000;140:153–160. [PubMed: 11484484]

50. Booth CR, et al. A 9 Å single particle reconstruction from CCD captured images on a 200 kV electron cryomicroscope. J. Struct. Biol 2004;147:116–127. [PubMed: 15193640]

51. Ludtke SJ, Baldwin PR, Chiu W. EMAN: semiautomated software for high-resolution single-particle reconstructions. J. Struct. Biol 1999;128:82–97. [PubMed: 10600563]

52. Brink J, et al. Experimental verification of conformational variation of human fatty acid synthase as predicted by normal mode analysis. Structure 2004;12:185–191. [PubMed: 14962379]

53. Ludtke SJ, Chen DH, Song JL, Chuang DT, Chiu W. Seeing GroEL at 6 Å resolution by single particle electron cryomicroscopy. Structure 2004;12:1129–1136. [PubMed: 15242589]

54. Pettersen EF, et al. UCSF Chimera—a visualization system for exploratory research and analysis. J. Comput. Chem 2004;25:1605–1612. [PubMed: 15264254]

55. Eramian D, et al. A composite score for predicting errors in protein structure models. Protein Sci 2006;15:1653–1666. [PubMed: 16751606]

56. Topf M, Baker ML, Marti-Renom MA, Chiu W, Sali A. Refinement of protein structures by iterative comparative modeling and CryoEM density fitting. J. Mol. Biol 2006;357:1655–1668. [PubMed: 16490207]

57. Jiang W, Baker ML, Ludtke SJ, Chiu W. Bridging the information gap: computational tools for intermediate resolution structure interpretation. J. Mol. Biol 2001;308:1033–1044. [PubMed: 11352589]

58. Van Der Spoel D, et al. GROMACS: fast, flexible, and free. J. Comput. Chem 2005;26:1701–1718. [PubMed: 16211538]

## Supplementary Material

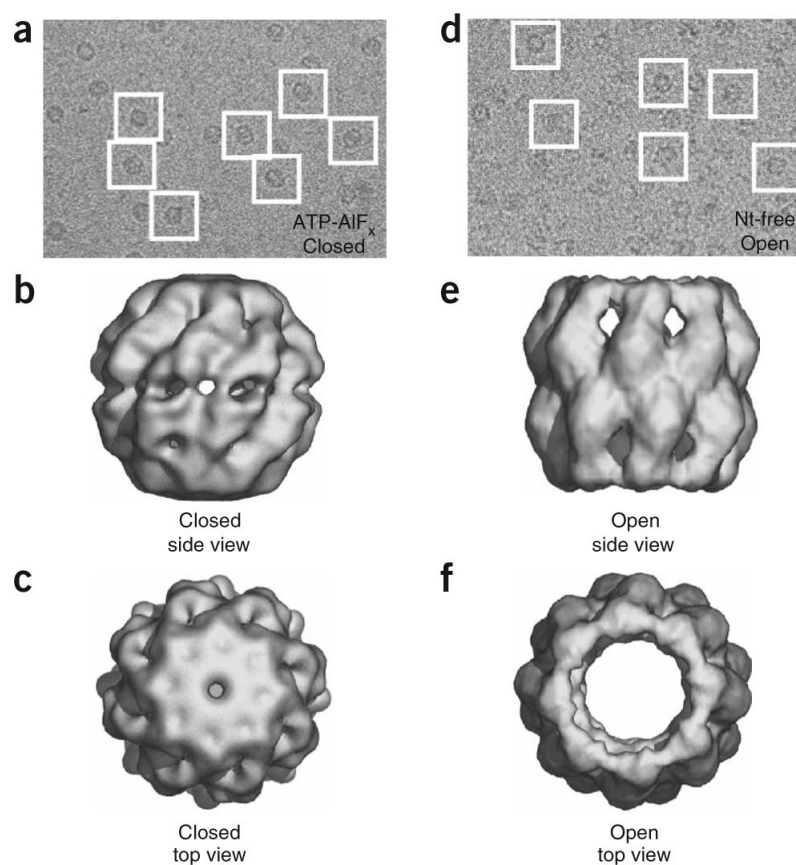Refer to Web version on PubMed Central for supplementary material.

**Figure 1.**
Cryo-EM density maps of the eukaryotic chaperonin TRiC in its open and closed
conformations. (**a**) A representative area of a CCD-captured image of ice-embedded TRiC in
the closed state, generated by incubation with ATP and AlF$_x$. (**b,c**) Side and top views of a
single-particle reconstruction of TRiC in its closed state, carried out with 7,129 particles to
~15-Å resolution. (**d**) A representative area of a CCD-captured image of ice-embedded open-
state, nucleotide-free TRiC. (**e,f**) Side and top views of a single-particle reconstruction of TRiC
in its open state, carried out with 13,287 particles to ~18-Å resolution.

α subunit model,
closed state

Subunit model versus
EM closed state

Top view

Side view

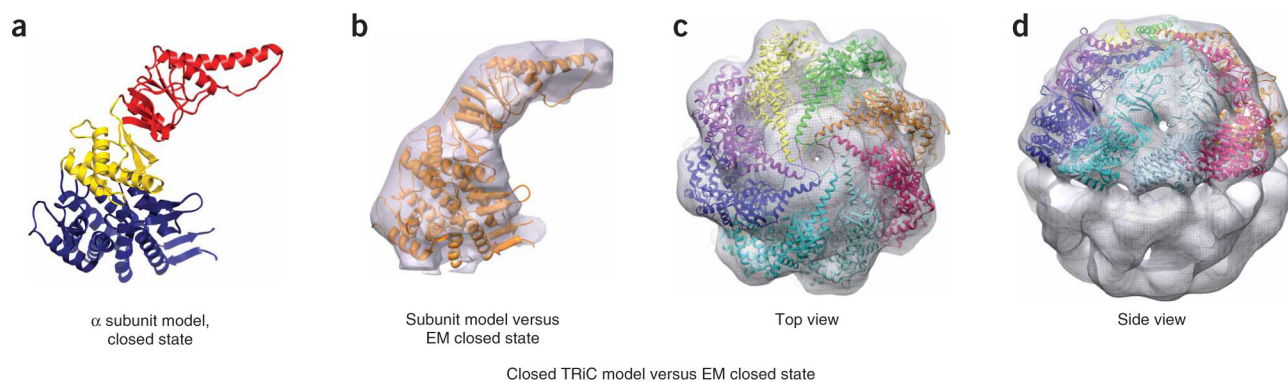Closed TRiC model versus EM closed state

**Figure 2.**
Comparative protein structure modeling the closed state of TRiC. (**a**) Homology model of the TRiC α subunit in the closed state. The apical domain is red, the intermediate domain is yellow and the equatorial domain is blue. (**b**) Fit of the TRiC α subunit model into the cryo-EM density map corresponding to a monomer of the closed state. (**c,d**) Top and side views of the homology model of closed TRiC docked into the cryo-EM density map. The fit has a similarity score of 0.987.
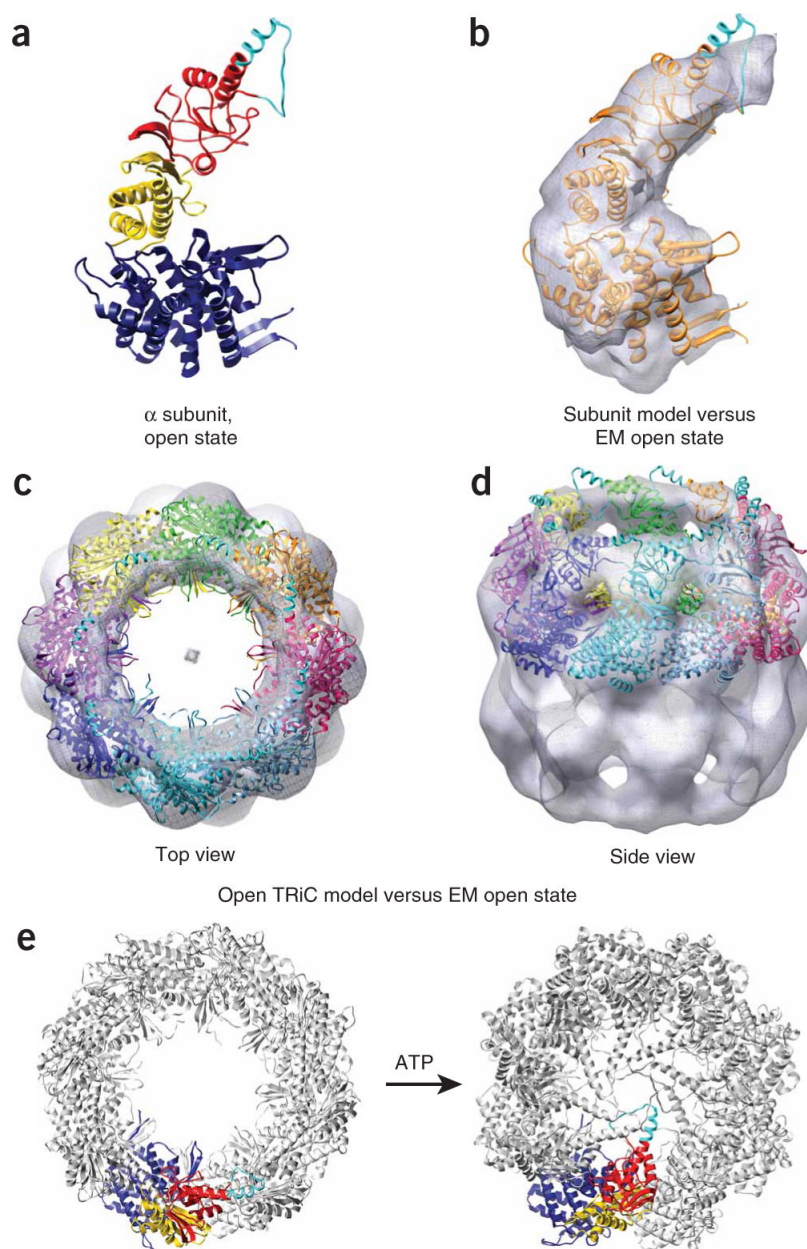
**Figure 3.**
Comparative protein structure modeling the open state of TRiC. (**a**) Homology model of the
TRiC α subunit in the open state. The apical domain is red, the intermediate domain is yellow
and the equatorial domain is blue. The short apical segment that forms the lid in the closed
state is highlighted in cyan. (**b**) The fit of the TRiC α subunit into the density map corresponding
to a monomer of the open conformation. The short apical lid segment is absent in the open-
state map, probably owing to its dynamic nature. (**c,d**) Top and side views of the open TRiC
model docked into the open-state cryo-EM density map. The fit has a similarity score of 0.969.
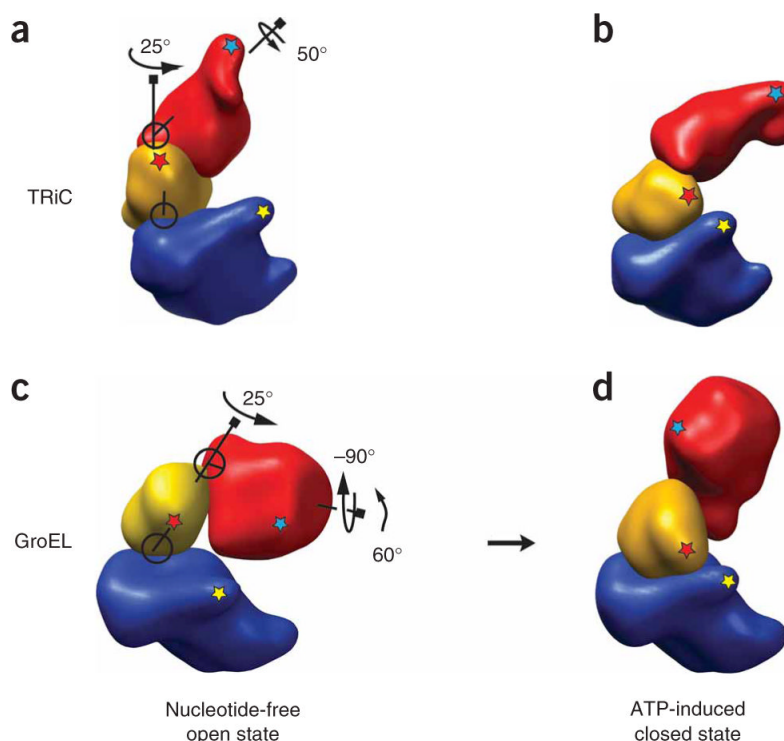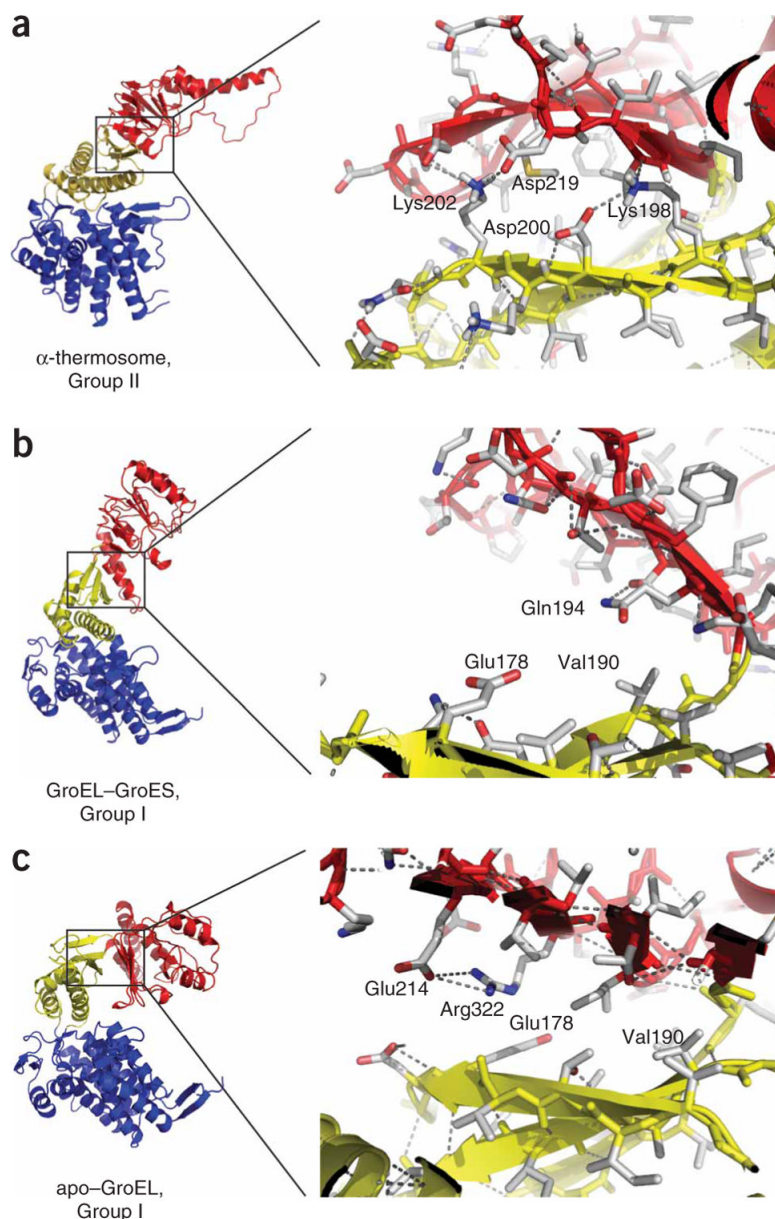(**e**) Top view of the ATP-driven open-to-closed transition in TRiC.

**Figure 4.**
Comparison of the conformational changes of TRiC and GroEL subunits. (**a,b**) Low-resolution representations of the TRiC subunits in the open, nucleotide-free (**a**) and closed, ATP-induced (**b**) conformations. The apical, intermediate and equatorial domains are shown in red, yellow and blue, respectively. Arrows indicate the direction and magnitude of proposed domain motions during lid closure. The intermediate domains rotate about ~25° toward the equatorial domain; the apical domains undergo a rotation of ~50° toward the equatorial domain accompanied by a lateral rotation of ~50° into the central chamber. Stars mark the fixed positions in each domain to facilitate visualization of relative domain movements. (**c,d**) Low-resolution representations of a GroEL subunit in the open (nucleotide-free)[30] (**c**) and closed (nucleotide-bound and GroES-bound)[30] (**d**) conformations, colored as in **a,b**, with stars marking fixed positions in each domain, as above. Arrows show the domain motions upon nucleotide and GroES binding. The intermediate domains rotate about ~25° toward the equatorial domain; the apical domains undergo a rotation of ~60° away from the equatorial domain accompanied by a lateral rotation of ~90° away from the central chamber.

**Figure 5.**
Apical-intermediate domain interfaces from crystallographic structures of the thermosome and GroEL. (**a**) The α subunit of the TRiC-like chaperonin called the thermosome[25]. The apical domain is red, the intermediate domain is yellow and the equatorial domain is blue. Inset, (viewed reversed relative to the subunit figures on the left) the contacts between the apical and intermediate domains are highlighted. (**b,c**) GroEL subunit in its closed, GroES-bound[30] (**b**) and open, unliganded[30] (**c**) conformations, with domains colored as for the thermosome. Insets (viewed reversed relative to the subunit figures on the left) indicate the lack of contacts between the apical and intermediate domains in either state.